Longitudinal dispersion within a two-dimensional turbulent shear flow

By PAUL J. SULLIVAN†

Department of Applied Mathematics and Theoretical Physics, Cambridge

This paper describes some laboratory and numerical experiments made on the longitudinal dispersion in an open channel flow. Particular attention has been paid to the initial stages of the process.

Physical arguments suggest that the streamwise dispersion of a line of marked fluid elements across a two-dimensional turbulent shear flow occurs in three distinct stages. These stages are identified by a change in the form of the distribution of marked fluid elements in the flow direction. The skewed distribution of the first stage is readily identified by a constant value (approximately $1 \cdot 1$) for the ratio of the peak velocity (V_1) of the distribution to the mean-flow velocity $\overline{U}$; experiments using dyed fluid, made at this stage of the process, have revealed six identifiable features of the suggested distribution. The distributions suggested for the second and the third stage are consistent with the experimental findings of Elder (1959) for the second stage and Taylor (1954) for the third stage.

An attempt has been made to simulate the process numerically using a Markovian model. The results of the simulation confirm features suggested by physical arguments and are in agreement with the open channel experiments.

The Lagrangian autocorrelation function is found to be related to the Lagrangian velocity-history of marked fluid released from extreme positions on the flow cross-section. The correlation function, as expressed in terms of the velocity-history function provided by the numerical simulation, is

$$R(t') = \exp\left(-bt'\right) \int_0^1 U^{+2} dy';$$

$$t' = t u_*/d, \quad U^+ = \frac{U(y') - \overline{U}}{u_*},$$

where u_* is the friction velocity and $U(y')$ is the temporal mean velocity at a (non-dimensionalized) distance y' from the flow boundary. In an open channel flow at a Reynolds number (based on friction velocity and channel depth) of 500, the numerical simulation provides the value of $b = 0 \cdot 536$.

The results of an experiment, in which the three-dimensional motion of small neutrally buoyant spheres was recorded in many small discrete time intervals, corroborate the theoretical suggestions and simulation results.

† Present address: Department of Applied Mathematics, University of Western Ontario, London, Ontario, Canada.

1. Introduction

A line of passively-marked fluid elements extending across a two-dimensional turbulent shear flow becomes dispersed in the streamwise direction primarily because of the variation in the mean velocity $U(y)$. Turbulent cross-stream mixing reduces this primary contribution to longitudinal spreading. The dispersive effects of molecular motion and of streamwise turbulent motion can be neglected (excepting particular regions of the flow cross-section, cf. Elder (1959) and §2.4) with respect to the main dispersive mechanism.

A kinematic formulation for the rate of growth of the second moment of a cloud of marked fluid, relative to a co-ordinate system moving at a velocity $\overline{U}$, has been given by Taylor (1921, 1954) who showed that

$$\frac{d\overline{X^2}}{dt} = 2\int_0^t \overline{U'(t)U'(t+\tau)}\,d\tau, \tag{1}$$

where $X = x - \overline{U}t$, and $U' = u - \overline{U}$; u is the streamwise velocity of a marked fluid element, and the overbar is used to denote an ensemble average of the marked elements of the cloud. Batchelor pointed out (see Taylor 1954; or Batchelor, Binnie & Phillips 1955) that the velocity of any marked fluid element released in a steady uniformly bounded shear flow ultimately will be independent of the release position and thus eventually become a stationary random function of time. Hence, following a sufficiently large time interval, say $t > T$, it follows that $\bar{u} = \overline{U}$, $d\overline{X^2}/dt = 2A$, where A is constant and

$$p(X, t) = 2(\pi A t)^{-\frac{1}{2}}\exp\left(-X^2/4At\right).$$

$p(X, t)$ is the probability-density function for marked fluid elements released from the plane $X = 0$ at $t = 0$. It would be difficult in practice to make direct measurements of the correlation function (1) because of the large value of T for which the fluid elements must be observed. In §4.2 a method is discussed in which this difficulty may, to a large extent, be circumvented. For flow in a smooth-walled pipe of radius a, Taylor (1954) gave an estimate of $10\cdot1\,au_*$ for A which he deduced from the solution of the diffusion equation

$$\frac{\partial}{\partial r}\left(\epsilon r\frac{\partial c}{\partial r}\right) = r\left(U(r)\frac{\partial c}{\partial x} + \frac{\partial c}{\partial t}\right).$$

The value of ϵ, the coefficient of radial transfer, in this equation was chosen by recourse to the Reynolds analogy. Taylor's estimate of A was in general agreement with his experimental findings if we choose $T \approx 15a/u_*$. But the distances at which this information becomes relevant are seldom reached in practice.

For $t < T$, direct account must be taken of the position of release of marked fluid on the flow cross-section. For the approximate interval

$$4d/u_* < t < 9d/u_*,$$

Elder observed a skewed distribution of dyed fluid in an open channel flow of depth d. He ascribed the long upstream tail to the retentive effects of the viscous layer and suggested the distribution could be discussed in two parts: a forward

Gaussian distribution representing dyed fluid over the major part of the cross-section, and a second Gaussian distribution representing dyed fluid in the viscous layer. Elder's experiments show that the peak value of the forward Gaussian distribution has a constant velocity approximately equal to $\overline{U}$, and that the second moment of the forward distribution increases linearly with time. This interesting result of Elder suggests that, with regard to the velocities of marked fluid elements released in the main body of the fluid, the state of the flow is very nearly stationary in a statistical sense. One object of the present work is to describe in detail the dispersion process for $t < T$: observations of a dispersing dye pulse (see, for example, figure 1, plate 1) suggest that it may be convenient to extend Elder's idea and divide the cross-section of the flow into a larger number of regions of longitudinal dispersion. Such a separation will have to be made on the basis of the local structure of the dispersing flow.

2. Three-stage description

2.1. *Physical arguments*

For $t > T$, the dispersion process is described by an effective longitudinal diffusivity A which depends upon the advective effects of the mean-flow velocity field, represented by $\overline{U}d$, and on the cross-stream mixing arising from the fluctuating velocity field. This later quantity is specified by u_*d and hence, on dimensional grounds,

$$A/\overline{U}d = f(\overline{U}d/u_*d). \tag{2}$$

Similarly the longitudinal diffusivity in laminar flow may be expressed in the form

$$A_L/\overline{U}d = f(\overline{U}d/k),$$

where k is the molecular diffusivity, and Taylor (1953) showed that

$$A_L/\overline{U}d = (1/48)\overline{U}d/k,$$

for flows in a pipe of radius d. Since the role of u_*d in (2) (i.e. cross-stream diffusivity) is the same in turbulent flows as that of k in laminar flows, one expects a similar linear relationship for the turbulent case, viz.

$$A/\overline{U}d = B\overline{U}/u_* \tag{3}$$

or

$$A = B(\overline{U}d)^2/u_*d.$$

In both the laminar and turbulent flows, $A/\overline{U}d$ is given as the ratio of two diffusivities. Thus it appears that the longitudinal dispersion is governed by the ratio of advective effects to cross-stream mixing.

If this concept applies to local regions of the flow, then there will be considerable variations in the longitudinal dispersion over the flow cross-section. For $t < T$ one is concerned with the local behaviour of the longitudinal dispersion, and to this end an attempt has been made to relate the local longitudinal dispersion to a co-ordinate system moving with the local velocity of the fluid $U(y)$. Consider the cross-stream diffusivity to be given by vL, where v is the local root-mean-square value of the cross-stream velocity and

$$L = \int_0^d \overline{\{w(y)w(\lambda)/\overline{(w(y)^2)}^{\frac{1}{2}}\,\overline{(w(\lambda)^2)}^{\frac{1}{2}}\}}\,d\lambda.$$

L is termed the local Eulerian length scale; $w(y) = u(y) - U(y)$. Relative to the moving observer the advective dispersion is $\delta U \delta y$, where δy is the cross-stream separation of two adjacent regions of fluid. A *local* dispersion coefficient can be expressed as $D(y) = c(\delta U \delta y)^2/vL$. To represent $D(y)$ graphically let $\delta U = (dU/dy)\delta y$ and let the constant, small increment, δy^2, be included in the (now dimensional) constant c such that $D(y) = (dU/dy)^2/vL$.

Townsend (1956) suggested that for sufficiently high Reynolds number the forms of $U(y)$, v and L for pipes and ducts will be universal and thus similar conclusions should apply to open channel flows. The following forms are a reasonable approximation to the measured values of Laufer (1951), in a duct of high aspect ratio, at Reynolds numbers of 12000, 30000 and 60000:

$$\left.\begin{aligned}
v/u_* &= (-0\cdot017y/d + 0\cdot04)f(R_*); \quad R_* = u_* d/v; \\
U(y)/u_* &= 2\cdot43\ln(y/d) + f(R_*); \\
f(R_*) &= 2\cdot43\ln(R_*) + 4\cdot9; \\
L/d &= 0\cdot21 \quad \text{for} \quad 0\cdot5 < y/d < 1.
\end{aligned}\right\} \quad (4)$$

A further assumption is made that $L = 0\cdot41y$ for $y_* < y < 0\cdot5d$, where

$$y_* = 30d/R_*$$

is the depth of the viscous layer. The viscous layer is neglected here and is discussed in §2.2.

The local dispersion $D(y)$ is shown on figure 2 for the (typical) value of $f(R_*) = 20$. Two distinct regions of variation in $D(y)$ occur on the flow cross-section. In the upper portion of the flow (approximately $y > \frac{1}{2}d$) $D(y)$ has a *low uniform* value, thereby indicating relatively strong cross-stream mixing, weak advection in the streamwise direction and, as a result, relatively large concentrations of marked fluid elements. Below this layer $D(y)$ rapidly increases as the solid boundary is approached. A large value of $D(y)$ indicates that the effect of advection is locally dominant and that the marked elements will accordingly be spread over a large streamwise span. It remains to assess the consequences of these subdivisions on the distribution $p(X, t)$, where

$$p(X, t) = \int_0^\infty \int_0^d c(X, y, z, t)\, dy\, dz \bigg/ \int\int_0^\infty c\, dX\, dy\, dz. \quad (5)$$

$c(X, y, z, t)$ is the concentration of marked fluid elements.

2.2. *Three-stage model*

The first stage refers to the period of time shortly after the release of marked fluid, during which a typical fluid element, released in the upper layer, has had time to sample the variation in flow properties within this layer, but the interval should be short enough that there is no significant flux of marked fluid from this layer. Because $D(y)$ is uniform in this region the streamwise spread of marked fluid, relative to the moving observer, is independent of y. Thus

$$\int_{\frac{1}{2}d}^d c\, dy$$

will be symmetric about a co-ordinate system moving with the constant mean velocity

$$V_1 = (2/d) \int_{\frac{1}{2}d}^{d} U(y)\, dy,$$

where from (4) $V_1/\overline{U} \approx 1{\cdot}10$ for $200 < R_* < 800$.
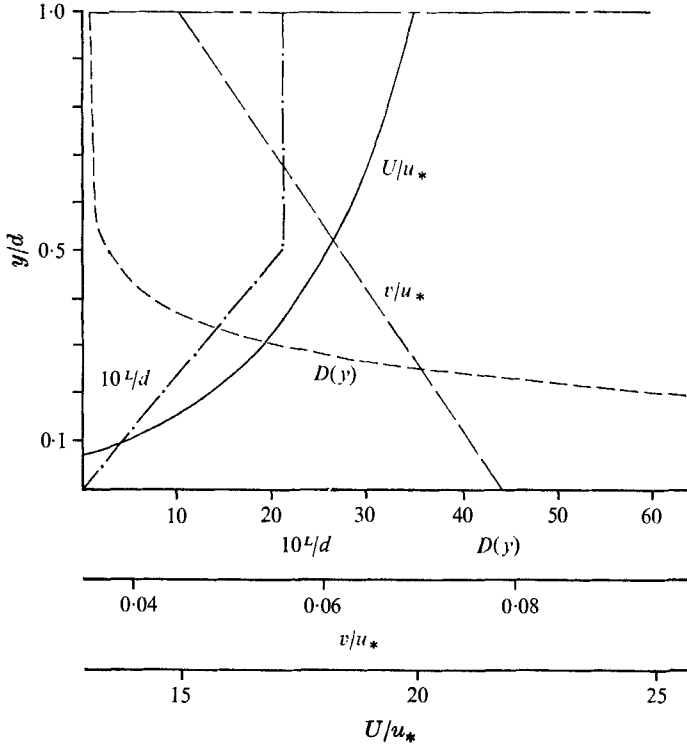
FIGURE 2. Typical variation in U, v, L, $D(y)$ across a two-dimensional bounded turbulent shear flow (viscous layer omitted).

The dominance of cross-stream mixing within this layer suggests that marked fluid released in, and remaining in, the layer would soon sample the variation existent within the layer, and its motion accordingly become independent of the release position. The symmetrical curves describing the streamwise distribution of these marked elements may be expected to settle down fairly rapidly to a Gaussian form. The longitudinal dispersion of these elements can be characterized by an effective non-dimensional diffusivity, $A_1 = D_1/u_* d$, where D_1 is the value of the longitudinal dispersion in this layer. Marked fluid migrating to the lower layer, $y < \frac{1}{2}d$, is rapidly advected upstream (relative to the moving observer) as a result of the high values of $D(y)$ in the lower layer. Hence the forward part of $p(X,t)$ describes marked fluid particles that are exclusively resident in the region $y > \frac{1}{2}d$. Because of the relatively low value of $D(y)$ for $y > \frac{1}{2}d$, the skewed distribution $p(X,t)$ has a dominant downstream Gaussian portion. Since there is a net flux of marked fluid from the downstream-upper

region of the flow cross-section, the modal value of $p(X, t)$ during the first stage diminishes at a rate faster than the $t^{-\frac{1}{2}}$ rate that would occur in a system with no overall mass efflux.

The second stage refers to a time interval during which marked fluid, released in the region $y > y_*$, has had time to sample the flow variation within this region, and before a significant flux of marked fluid *into* the viscous layer has occurred. The dominant forward feature of $p(X, t)$ during the first stage diminishes because of longitudinal dispersion within the upper layer, and through the flux of marked

Property	1st stage	2nd stage	3rd stage
Form of $p(x, t)$	A_1	$\quad < \quad$ A_2	$\quad < \quad$ A_3
Di/u^*d	~ 0.2 open channel	~ 5 open channel	~ 11 (pipe)
Area described by Gaussian	$\frac{1}{2}d < y < d$	$y^* < y < d$	$0 < y < d$
Peak decay rate	$> t^{-\frac{1}{2}}$	$> t^{-\frac{1}{2}}$	$t^{-\frac{1}{2}}$
Peak to mean velocity ratio	~ 1.10	~ 1.02	1
Approximate time of relevance	$tu^*/d > 0.5$	$tu^*/d > 4$	$tu^*/d > 30$
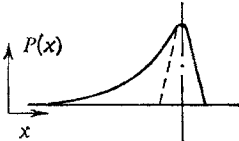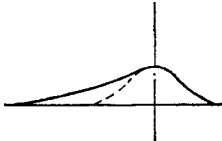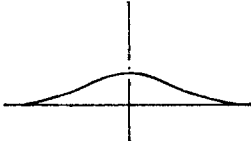
TABLE 1

fluid out of the forward part of this layer. Subsequently the modal value of $p(X, t)$ occurs upstream (e.g. closer to the centre of gravity of the dispersing cloud) relative to that of the first stage. During the second stage, the distribution of marked fluid about a co-ordinate system moving with a velocity

$$V_2 = \frac{1}{d - y_*} \int_{y_*}^{d} U(y)\, dy$$

(i.e. slightly in excess of $\bar{U}$) is Gaussian and the dispersion of this fluid is characterized by an effective longitudinal diffusivity $A_2 = D_2/u_* d$, where D_2 is the value of the longitudinal dispersion in this layer (viz. $y_* < y < d$).

The advective effects of the viscous layer translate migrant marked fluid from $y > y_*$ upstream, relative to the forward part of the dispersing cloud. Thus $p(X, t)$ is skewed in the second stage with a dominant downstream Gaussian section resulting from marked fluid particles residing in the region $y > y_*$. As in the first stage the modal value diminishes faster than it would in a bound system because of the flux of marked fluid into the viscous layer.

Finally, in the third stage, all of the marked fluid has sampled the entire flow cross-section, including the viscous layer, and $p(X, t)$ is a Gaussian distribution relative to a co-ordinate frame at the position $x = \bar{U}t$. A non-dimensional diffusivity $A_3 = D_3/u_* d$ then describes the longitudinal dispersion taking place

over the entire cross-section and the modal value of $p(X, t)$ diminishes at a rate proportional to $t^{-\frac{1}{2}}$. The effective longitudinal diffusivity in the three stages describes fluid encountered in regions of the flow with successively higher values of $D(y)$ and as a result $A_1 < A_2 < A_3$. The values of A_i are expected, by (3), to be linear functions of $(\overline{U}/u_*)^2$, except for hydraulically rough flows where, for a given roughness and sufficiently large R_*, $(\overline{U}/u_*)$ is a constant.

The three stages refer to three distinct forms of $p(X, t)$ which arise from the successive importance of three areas of the flow cross-section, so chosen because of their differing ability to disperse marked fluid in the streamwise direction. The successive dominance of $p(X, t)$ by marked fluid within the three areas leads to these three distinct stages. Some details of the three stages may now be compared with experimental data. A summary of the distinguishing features of each stage is given in table 1 with the time of relevance of each description approximated from the data of Elder (1959), Taylor (1954), and from the experimental results of §2.4.

The experimental results of Elder (cf. §3) agree with the description of the second stage of the process: for flow in an open channel these results suggest that $A_2 \simeq 5$. Taylor (1954) and Batchelor *et al.* (1955) confirm the foregoing description of the third stage. Taylor, however, suggests that the value of A_3 for a pipe flow is independent, for sufficiently high values, of the Reynolds number. The second and third stage descriptions are consistent with experimental evidence, except for the dependence of A_3 on R_* which has not yet been properly verified (cf. §3.3); it thus remains to compare the first-stage description with experimental observations.

2.3. *Experimental investigation*

The experiments described herein were made in an open channel of 8 m length and 0·8 m width. An experimental working section (2·45 m by 0·46 m) was set out between the growing side-wall boundary layers and beginning at the downstream position where the floor boundary layer extends over the flow depth. Measurements of $U(y)$, using a miniature current meter, indicate that the flow in the working section is two dimensional and is well represented by the boundary-layer expression,

$$U(y)/u_* = 2\cdot43 \ln (yu_*/\nu) + 4\cdot9,$$

which was suggested by Clauser (1956).

The 'marked fluid' used for these experiments was an aqueous solution of the dye Gentian Violet which was very nearly neutrally buoyant in water. This solution was injected through the free surface in the form of discrete, reproducible, pulses with sufficient momentum to penetrate the viscous layer. The initial column of dyed fluid (nominally 2·5 cm in diameter) would spread over about 150 cm along the working section. The dispersing dye clouds were photographed and the optical densities of the dyed fluid on the negatives determined by means of a Joyce microdensitometer (Elder describes this technique in detail) to obtain

$$C(x, t) = \frac{1}{Q} \int_0^d \int_0^\infty \overline{c(x, y, z, t)} \, dy \, dz$$

and
$$C(z,t) = \frac{1}{Q} \int_0^d \overline{c(x_1, y, z, t)} \, dy,$$

where
$$Q = \int c(x, y, z, t) \, dx \, dy \, dz$$

and c is the concentration of the dyed fluid. In this expression $x_1 = \overline{U}t$, with the overbar denoting an averaged value of c at t from the release of (nominally 7) similar pulses. It is assumed that $p(X, t) = C(X, t)$.

2.4. *Experimental results*

The relevant measurements made from six different flow conditions are listed in table 2. The experimental observations, taken for values of t such that

$$0.5 < tu_*/d < 4,$$

were found to coincide with the first stage description. The following itemization sets out the details for comparison with the foregoing description (cf. §2.2).
(i) The $C(x, t)$ are skewed, and a nearly Gaussian forward section is followed by a
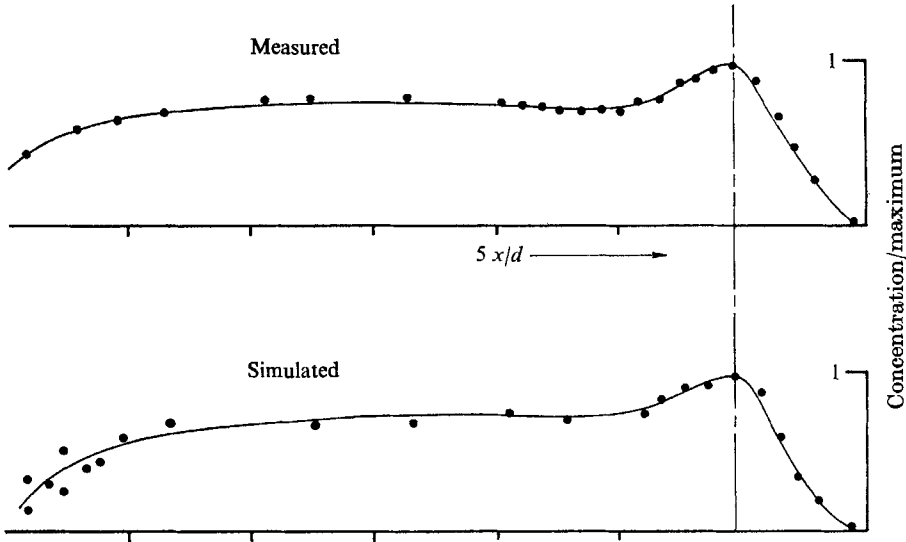
FIGURE 3. Simulated and experimental depth-integrated concentration at $R_* = 790$.

long upstream tail (cf. figure 3). (ii) The forward Gaussian section of $C(x, t)$ is associated with dyed fluid resident in the region $y \geqslant \frac{1}{2}d$. (iii) The second moment of the forward Gaussian section grows linearly with time. (iv) The constant of proportionality of item (iii), i.e. $A_1 = D_1/u_* d$, lies in the range $0.1 < A_1 < 0.3$. This is significantly less than the equivalent value of 4.61 found by Elder[†] for an open channel flow in the second stage. (v) A_1 appears to be a linear function of $(\overline{U}/u_*)^2$, (cf. figure 5). (vi) The peak velocity V_1 is a constant such that $V_1/\overline{U} \simeq 1.10$. The variation of V_1 over the range of Reynolds numbers used in these experiments

† Elder (1959) appears to have assumed the second moment to occur at $\frac{1}{2}$ the modal value of the Gaussian distribution. Corrected values are referred to throughout this paper.

is shown in table 2 and figure 6. (vii) The peak value appears to decay as $\exp(-0{\cdot}3t)$, i.e. more rapidly than $t^{-\frac{1}{2}}$.

The values of the non-dimensional lateral diffusivity are given in table 2. The average value of $0{\cdot}12$ is in reasonable agreement with the value of $0{\cdot}16$ found by Elder, if the low value of $R_* \sim 250$ used in Elder's experiments is taken into account.

If one makes the assumption that the additional contribution to the longitudinal diffusivity, arising from fluctuations in the streamwise velocity field, is approximately equivalent to the lateral diffusivity then this contribution to A_1 is not negligible.

In fact, for low values of R_*, one expects A_1 to be determined almost entirely by the streamwise velocity fluctuations; this contribution becomes relatively less important with increasing R_*.

The open channel experiments appear to confirm the first-stage description of the process. The most convincing agreement is in the experimental values of $V_1 \simeq 1{\cdot}10\,\overline{U}$. Moreover, as already indicated, the description of the second stage and the third stage are compatible with previous experimental observations, and hence the concept of a three-stage model provides a basis for the comparison of the experimental results with a numerical simulation of the dispersion process.

3. A simulation of the dispersive process

3.1. *Statistical model*

A simulation of the dispersion process is limited by a lack of available Lagrangian information. An attempt was made to simulate the process using the available Eulerian information in a pseudo-Lagrangian way. Thus a model akin to a random-walk process within a bounded region was constructed. Incorporated in the model were path lengths, fluctuating velocity scales, convective time scales and mean velocity scales that were functions of position. A digital computer was programmed to calculate the path of an initially prescribed particle position (i.e. 'a marked element') as it proceeded through the statistical field variables. Many such paths were used to compile a probability distribution by means of an ensemble average.

Fluid elements at a cross-stream position y are convected in the y direction with a velocity that is a statistical function of its position. The duration of influence of this velocity is also a statistical function of y. The elements travel through positions of differing mean velocity and accordingly there is a simultaneous streamwise spread of dye. For the purpose of the simulation, the streamwise velocity fluctuations were neglected and elements placed at y were considered to have a velocity v and to be convected to a time interval L/v in an upward or downward direction relative to the mean motion. This latter process was assigned randomly and is the only random element in the model.

This model assumes that fluctuating components exist, on average, for the time of one 'eddy cycle' and that the statistical functions of time scales, length scales, and velocity scales may be replaced by their mean values. It is anticipated, since many marked elements pass through these points on the

cross-section prior to compilation of their distribution, that an adequate representation can be realized in this way. No attempt was made to assume the statistical distributions of the variables since such added complexity would have been inconsistent with the approximate nature of the simulation.

The lower spatial bound was assumed to occur at the depth of the viscous layer, i.e. at y_*, and when a marked fluid element encountered a boundary the values of v and L were recalculated.

R	d[cm]	u^* [cm/sec]	R_*	$\overline{U}$ [cm/sec]	E	Largest error	A_1	A_1 (lateral)
8550	13·7	0·403	500	7·18	1·075	0·02	0·085	
10250	13·1	0·500	582	8·93	1·093	0·02	0·130	
11950	12·1	0·619	665	11·2	1·110	0·02	0·220	
13650	10·2	0·826	750	15·3	1·100	0·05	0·260	0·108
14350	8·95	0·990	784	18·5	1·122	0·02	0·293	0·110
14500	7·32	1·21	790	22·9	1·125	0·05	0·295	0·133

$R = \overline{U}d/\nu$, $E = V_1/\overline{U}$. Largest error represents ratio of most distant reading from the mean to the mean value of E. A_1 (lateral) $= \frac{1}{2}\overline{dZ'^2}/dt$; $Z' = Z/d$, $t' = tu_*/d$, $Z =$ lateral co-ordinate distance.

TABLE 2

3.2. *Simulation*

In the simulation the marked elements were given a cross-stream velocity appropriate to their position, and were allowed to travel for a time $\tau = L/v$. The resulting displacement at the end of this time interval has the components

$$\Delta x = L/v \int_{y_1}^{y_2} U(y)\,dy,$$

$$\Delta y = \pm Lv/v = \pm L.$$

At the next position $y = y + \Delta y$, $x = x + \Delta x$, the values of v, L and τ were selected for the new values of y and again a random sign was attached to v. This procedure was repeated for the desired time and for sufficiently large numbers of marked elements to give a reliable ensemble average of the final distribution.

Length scales and velocity scales in the simulation were non-dimensionalized using the depth and the friction velocity respectively. Thus $x' = x/d$, $y' = y/d$, $L' = L/d$, $v' = v/u_*$, $\overline{U}' = \overline{U}/u_*$. The time variable was non-dimensionalized as $t' = tu_*/d$ and the process was characterized by one parameter – namely R_*. The universal forms of U, L, v (see §2.1) were used together with the assumptions

$$U'(y) = 2\cdot5 \ln(y') + f(R_*), \quad \text{pipe or duct};$$

$$f(R_*) = 2\cdot5 \ln(R_*) + 5\cdot5;$$

and $\qquad L' = y' \quad \text{for} \quad y' < 0\cdot2; \; L' = 0\cdot21 \quad \text{for} \quad 1 < y' < 0\cdot2.$

$p(x', y', t')$ is the probability density function describing the position of marked fluid elements over the flow cross-section following their release from the plane

$x' = 0$. Generally, 5000 marked elements were uniformly spread over the depth at $t' = 0$ on $x' = 0$. The streamwise probability density function is then

$$p(x', t) = \int_0^1 p(x', y', t') \, dy'.$$
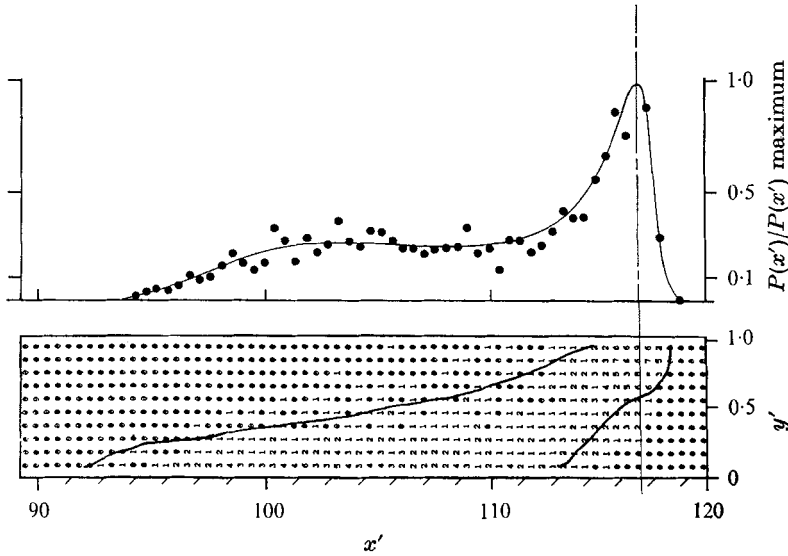
FIGURE 4. $P(x', y')$ and $P(x')$ at $tu_*/d = 3$, $R_* = 800$. $P(x\,y)$ $\theta = \theta \to 0.\theta5$; $1 = 0.\theta5 \to 0.15$; $2 = 0.15 \to 0.25$; etc. $* = 0.95 \to 1$.
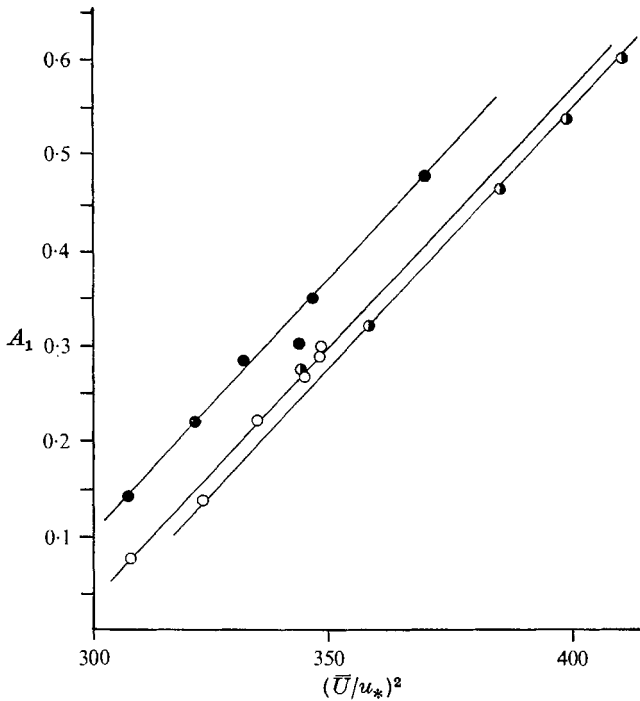
FIGURE 5. First-stage dispersion coefficient. $\bigcirc$, experiment; $\bullet$, simulation of channel; $\lefthalfblack$, simulation of pipe or duct.

3.3. *Simulation results*

The form of $p(x', t')$ in the simulation, during the first stage of the dispersion process, agrees with the experimental observations of § 2.4. In figure 4 a graph of $p(x', y', t')$ shows that the forward Gaussian part of $p(x', t')$ is associated with marked fluid residing in the region $y' > \frac{1}{2}$, as suggested in § 2.2 (and see figure 1). The simulated value of A_1 is compared in figure 5 with experimental results. The peak value diminishes approximately as $e^{-0.3t}$, in agreement with the experimental result.
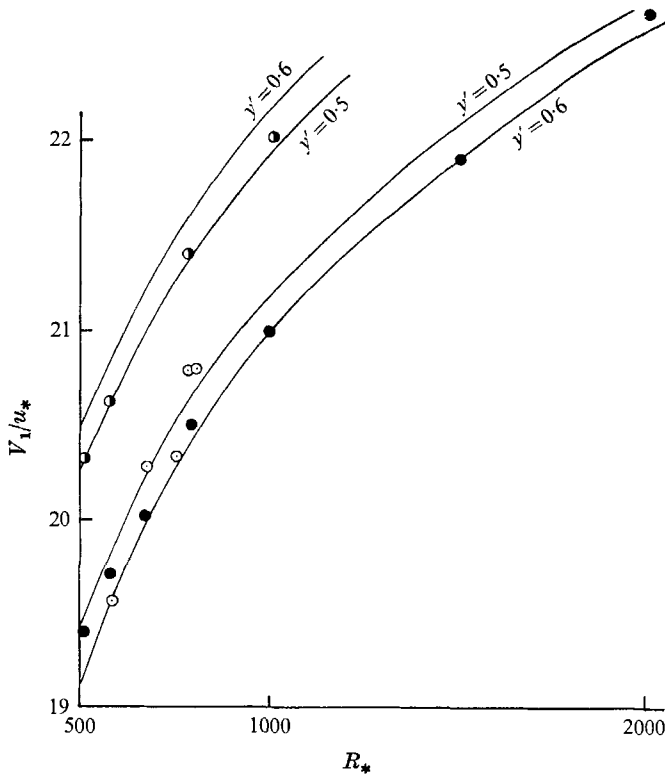
FIGURE 6. Velocity of modal value during first stage. Symbols same as figure 5.

$$\underline{\hspace{1cm}}, \quad \frac{1}{1-y'} \int_{y'}^{1} \frac{U}{u_*} \, dy' = f(R_*).$$

In figure 6 the variation of V_1 with R_*, found from the simulation, is compared with the experimental result. Also included in this graph are the results of calculations made with various lower bounds to the uppermost layer. From these calculations it is suggested that the lower bound of this layer lies between $y' = 0.5$ and $y' = 0.6$. Measurements of Bentley & Dawson (1966) indirectly verify this result. In their measurements the out-of-phase velocity between an input and a measured harmonic signal near the centre of a pipe flow was recorded. At $R_* = 700$ the out-of-phase velocity was found to be 112 % of the mean-flow velocity, and this percentage decreased with increasing R_*.

Slight modifications were made to the forms of the flow variables used in the simulation by altering the coefficients by 10 %. The forms of the resulting distributions were affected only by a very small amount, and in a predictable manner. The assumed variation of L' near the solid boundary was changed to $L' = 0.41y'$ at $y' < 0.5$ and this did not alter the value of A_1, thereby suggesting that the longitudinal dispersion in the upper layer is not directly dependent upon the structure of the lower layer.

In formulating the simulation process the role of a viscous layer was eliminated. The long tail of the skewed distribution produced in the first stage of the simulation was produced without recourse to an argument directly involving the viscous layer. This is in fact evidence for a distinctly different stage of the dispersive process from that described by Elder (1959).
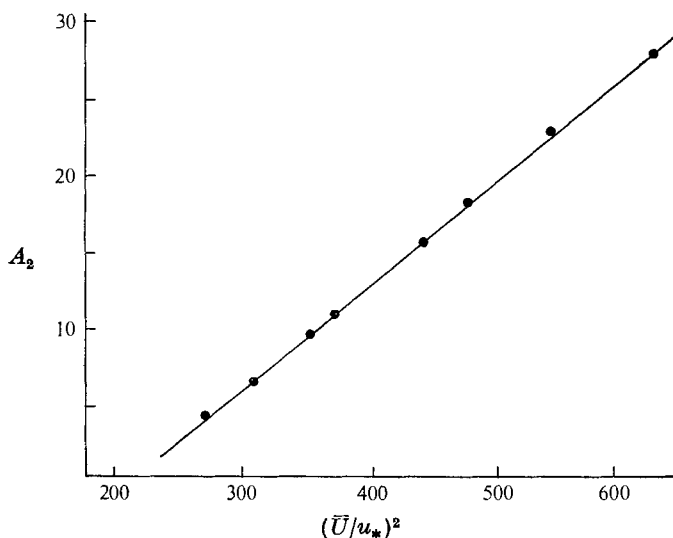
FIGURE 7. Simulation values of dispersion coefficient after large time.

The results of the simulation are in general qualitative agreement with the experimental observations of §2.4. The apparent quantitative agreement for A_1 is fortuitous: the streamwise fluctuating velocity was not included in the simulation and compensation for this fact would lead to the displacement of the simulated values of A_1 from the experimental values by an additional factor of 0.1 (cf. §2.4).

The dispersion process takes place within a bounded region $y_* < y' < 1$, and ultimately $p(x', t')$ becomes Gaussian about an axis moving with the mean velocity of this flow region. The longitudinal non-dimensional diffusivity of the simulation, at large times, should compare with A_2 of the second stage because of the elimination of the viscous layer from the simulation (cf. §2.2). Figure 7 shows the linear dependence of A_2 upon $(\overline{U}/u_*)^2$ and also that $A_1 < A_2$: these results are in qualitative agreement with the physical arguments of §2.2. The viscous depth decreases with R_* so that the second-stage diffusivity describes marked fluid over

a cross-section which is increasing with increasing R_*. The cross-sectional increase is caused by the addition of more flow area adjacent to the solid boundary where the local diffusivity is increasing (cf. §2.1). The difference between A_2 and A_3 decreases with increasing R_*, and the values of A_3 are less sensitive to changes in R_* than are the values of A_2.

The simulation provides a qualitative confirmation of the three-stage description and of the experimental observations of the dispersion process. One advantage of this simulation is that it does not formulate the process in terms of flux resulting from a concentration gradient, as would be the situation when using a 'mixing length' formulation.

4. Lagrangian statistics in a bounded turbulent shear flow

4.1. *Lagrangian mean histories*

In a homogeneous field of turbulence the Lagrangian statistics are independent of the release position, but the opposite is generally true in a turbulent shear flow. Although the length scales of the turbulent fluctuations may be reasonably
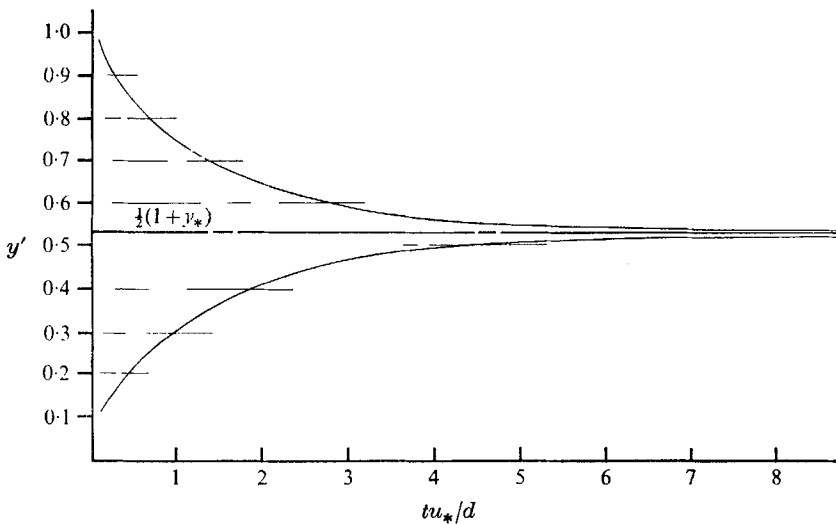
FIGURE 8. Simulation result for mean cross-stream position. $R_* = 500$.

small, these scales vary over the flow cross-section. This spatial variation leads to an exceptionally long period of time (or an equivalent streamwise length of flow) over which the motion of a marked fluid element must be recorded in order to compile these statistics.

Consider the mean path (projected on a vertical plane lying parallel to the mean flow) of elements starting at different positions of the flow cross-section. Ultimately, the mean paths for all release positions must be constant, i.e. $y = d$ for a pipe of radius d, a duct of half-depth d, or $y = \frac{1}{2}d$ for an open channel of depth d. Initially, for a short period of time, the mean path is a straight line, and thereafter it smoothly approaches its limiting value for large times. The length of

the straight-line segment depends upon the release position, and it terminates when a marked element, from a given release position, first reaches the boundary. For marked elements released near the centre of the cross-section the straight-line portion is longest. But even there it persists for a time which is short in comparison with the time required for the mean path of elements released at the boundary to reach their final value. Neglecting this small initial straight line
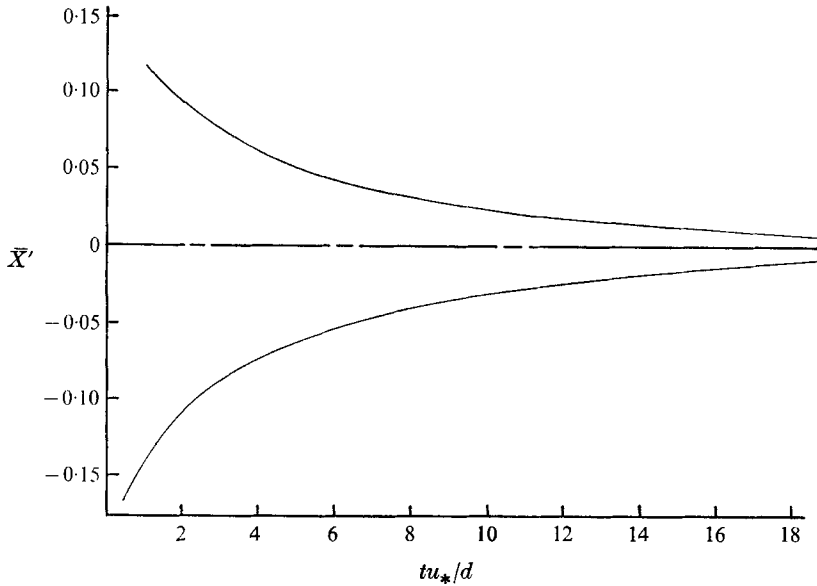

FIGURE 9. Simulation result for mean history of $\bar{X}'$. $R_* = 500$.
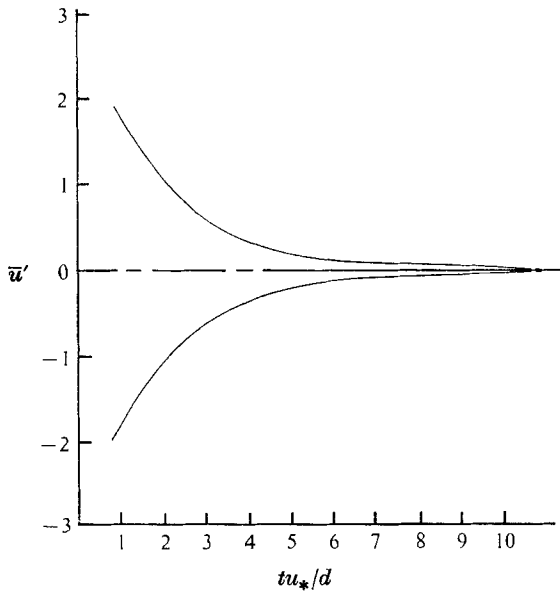
FIGURE 10. Simulation result for mean history of $\bar{u}'$. $R_* = 500$.
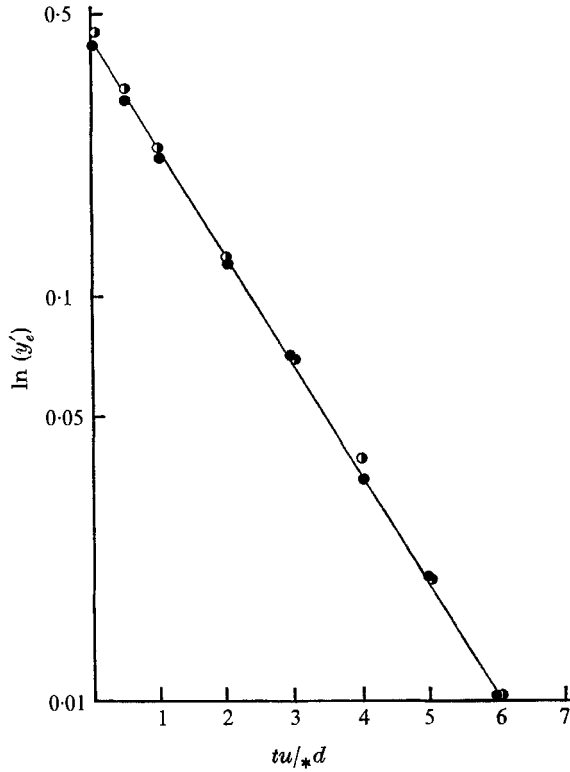
FIGURE 11. Simulation result. $R_* = 500$. $\bullet$, $y'_e = y' - \frac{1}{2}(1+y_*)$; $\mathbb{O}$, $y'_e = \frac{1}{2}(1+y_*) - y'$.
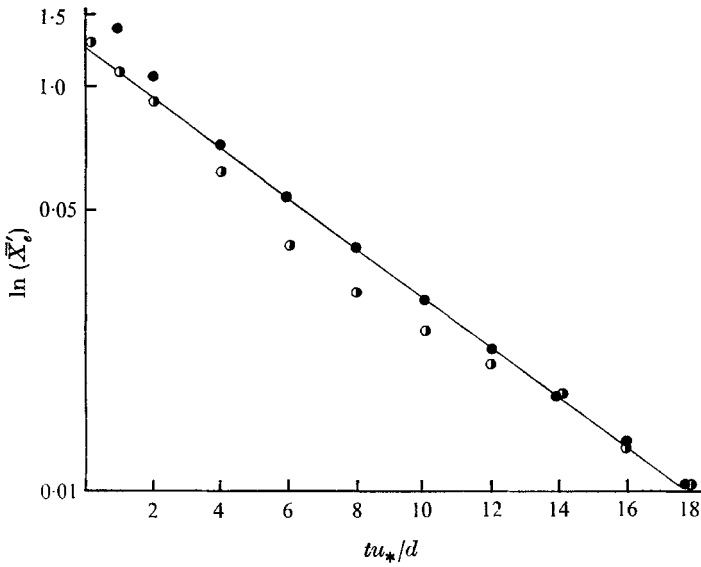
FIGURE 12. Simulation result. $R_* = 500$. $\mathbb{O}$, positive $\bar{X}'_e$ values; $\bullet$, negative $\bar{X}'_e$ values.

segment one expects the mean paths, for each release position on the flow cross-section, to be described by a part of the mean path for elements released at the flow boundaries (extremum paths). For example, the mean trajectory corresponding to a release position $y = 0\cdot8d$ in an open channel would be given by the segment
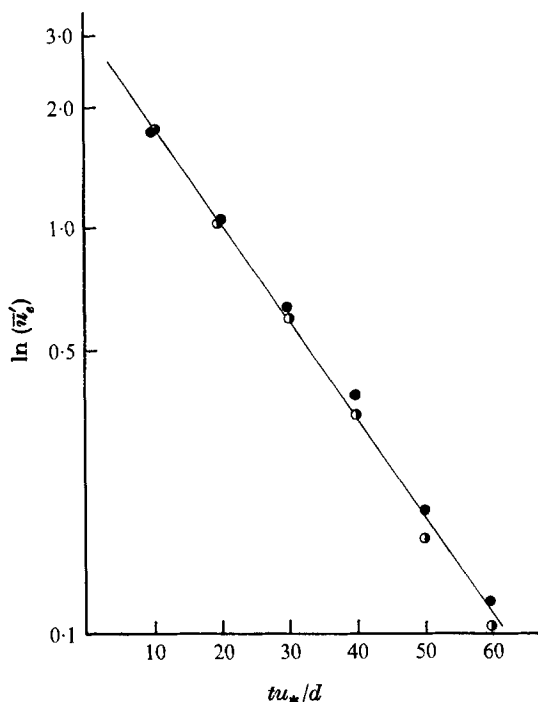
FIGURE 13. Simulation result. $R_* = 500$.
◑, positive $\bar{u}'_e$ values; ●, negative $\bar{u}'_e$ values.

of the extremum curve between $y = 0\cdot8d$ and $y = 0\cdot5d$ (see figure 8). A typical particle, released at approximately $y = d$ and subsequently arriving at $y = 0\cdot8d$, differs in future behaviour from elements released at $y = 0\cdot8d$ because the former arrives with a positive velocity and the latter has no such bias direction to its motion at the time of release. This difference is considered to be a small effect and is neglected by the exclusion of the straight line segments of the mean paths. The same principle applies to the ensemble mean histories of the random variables

$$X' = \frac{x - \bar{U}t}{d} \quad \text{and} \quad u' = \frac{u - \bar{U}}{u_*},$$

although the 'initially straight' description is not applicable to these variables. If one takes the Eulerian limit for small times following the release, the logarithmic variation of the mean flow field ensures that, although excursions in the cross-stream direction are equally probable, the resulting magnitudes of the streamwise velocities are *not* equally probable. Hence there results a net change in the Lagrangian ensemble mean value of the random variables X' and u'.

Figure 8, 9, 10 show the superposition of mean histories for release positions separated by $0\cdot1d$ intervals over the region $0\cdot1d < y \leqslant 0\cdot9d$.

For each position 1000 marked elements were used in an open-channel simulation; the Reynolds number R_* was 500. There appears to be no significant departure from the extremum curve when the curves for the various release positions are superposed, and in addition the extremum curves appear to be symmetrical. Figures 11, 12, 13 show that the (semi-logarithmic) plots of X', y' and u' against t' from which the following approximate expressions were derived:

$$\left. \begin{aligned} y'_e &= 0 \cdot 44 \exp\left(-0 \cdot 36 t'\right), \\ X'_e &= 0 \cdot 134 \exp\left(-0 \cdot 199 t'\right), \\ u'_e &= 2 \cdot 98 \exp\left(-0 \cdot 536 t'\right); \end{aligned} \right\} \tag{6}$$

the subscript e refers to the extremum curve.

The mean histories represent a loss of information relative to the initial release position, and the times taken for the extremum curves to reach the final value should correspond to the Lagrangian integrated time scale. Initially straight segments of mean paths were not noticeable in the simulation with the time intervals used ($\Delta t' = 0 \cdot 2$) to construct y'_e; their neglect is justified in the model.

4.2. *Lagrangian autocorrelation from the mean velocity history*

The correlation function $R(\tau) = \overline{u'(t')u'(t'+\tau)}$ can be constructed by taking an ensemble average of the velocities of marked elements released at uniform intervals over the flow cross-section, and then averaging the result recorded at the individual release positions. Arranging $R(\tau)$ into products of the mean U^+ and fluctuating u^+ components of the velocity u' there are only two non-zero terms. Thus

$$R(\tau) = \overline{U^+(t')U^+(t'+\tau)} + \overline{u^+(t')u^+(t'+\tau)}.$$

The second of these, the correlation of fluctuating velocities, is very much smaller than the first, (typically $u^+ \sim 0 \cdot 05 U^+$) and has a shorter correlation-time scale. Neglecting the second term, the correlation function for marked fluid elements, released at cross-stream position y'_1, is thus

$$R(y'_1, t') = \overline{U^+(y'_1, t')U^+(y'_1)},$$

where $U^+(y'_1, t)$ is the mean history of marked elements released at y'_1. In terms of the *extremum* curve found in §4.1 this becomes

$$R(y'_1, t') = U^+(y'_1) a \exp\left(-b T'\right),$$

where $T' = t' + t'_1$, with $t'_1 = \ln\left(U^+(y'_1)/a\right)/b$ for an extremum curve of the form $u'_e = a \exp\left(-b t'\right)$. To compile the average correlation function $R(t')$, made up from y'_1 evenly distributed over the flow cross-section, one integrates $R(y'_1, t')$ to obtain

$$R(t') = \int_0^1 R(y') \, dy' = \int_0^1 U^+(y') a \exp\left(-b T\right) dy'$$

$$= \int_0^1 a U^+(y') \exp\left(-b t'\right) \exp\left(\ln\left(U^+(y')/a\right)\right) dy'.$$

Thus
$$R(t') = \exp\left(-b t'\right) \int_0^1 U^+(y')^2 \, dy'. \tag{7}$$

The form of $R(t')$ could have been derived for some other random process (for example, correlating events described by a Poisson distribution). In fact, Taylor (1921) derived a similar correlation function to describe the dispersion of particles restricted to move in discrete single-value steps. In that study a correlation was assumed to exist between successive steps and, in passing to the limit of a continuous process, a correlation coefficient $R(t) = \exp(-t/N)$ was found, where

$$N = \lim_{\tau \to 0} [\tau/(1-g)]$$

and g is the correlation between two successive time steps. By analogy, the coefficient $1/b = 1/0.536$ in the expression derived from the simulation corresponds to N in the Taylor result.
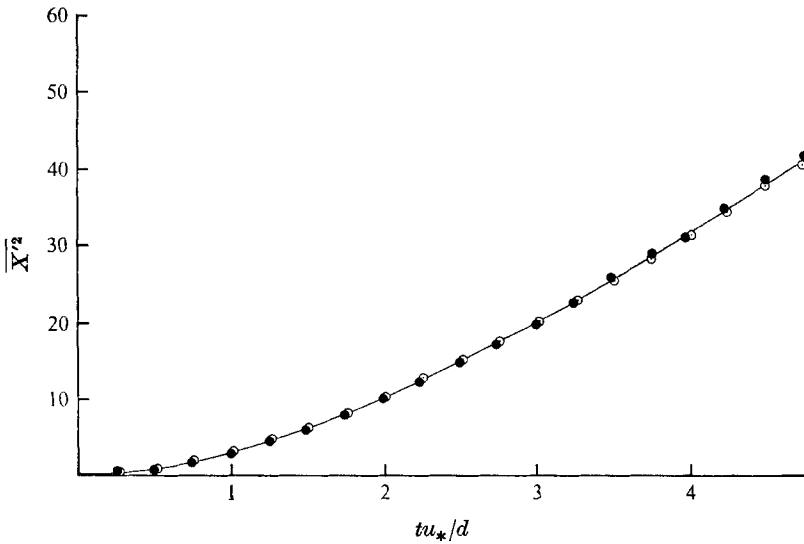
FIGURE 14. Simulation result at $R_* = 500$. $\odot$, equation (8) using $b = 0.536$ and y^* as limit of integration; $\bullet$, measured directly in simulation.

Taylor (1954) showed, for flow in a pipe, that the Lagrangian autocorrelation function is related to the growth rate of the second moment of a cloud of marked fluid particles. From Taylor's work

$$\frac{\overline{dX'^2}}{dt'} = 2\int_0^{t'} \overline{u'(t')u'(t'+\tau)}\,d\tau = 2\int_0^{t'} R(\tau)\,d\tau.$$

Using expression (7) for $R(\tau)$

$$\frac{\overline{dX'^2}}{dt'} = 2\int_0^{t'} \exp(-b\tau)\,d\tau \int_0^1 U^+(y')^2\,dy'$$

$$= (2/b)(1-\exp(-bt'))\int_0^1 U^+(y')^2\,dy'.$$

Hence $\qquad \overline{X'^2} = (2/b)[t'-(1/b)(1-\exp(-bt'))]\int_0^1 U^+(y')^2\,dy'. \qquad (8)$

P. J. Sullivan

The value of $\overline{X'^2}$ as a function of t' is compared in figure 14 with the values determined directly from simulation. The lower bound of the integral was chosen at y'_* so that the calculated values would be consistent with the simulation. At large t', $d\overline{X'^2}/dt'$ is a constant, and the derived expression attains 99·9 % of the asymptotic value when $t' = 7$. This is consistent with the results from the simulation. The non-dimensional diffusivity, A_3, of the third stage is given by

$$A_3 = (1/b) \int_0^1 U^+(y')^2 \, dy'.$$
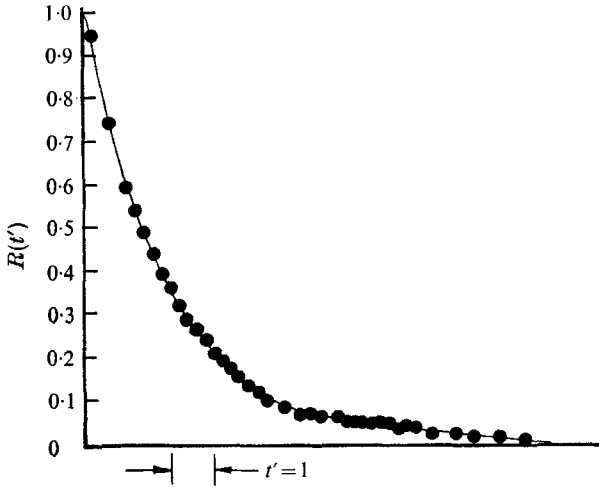
FIGURE 15. Simulation result compared with equation (7) at $R_* = 500$.
●, simulated values; —, exp $(-0·536t')$.
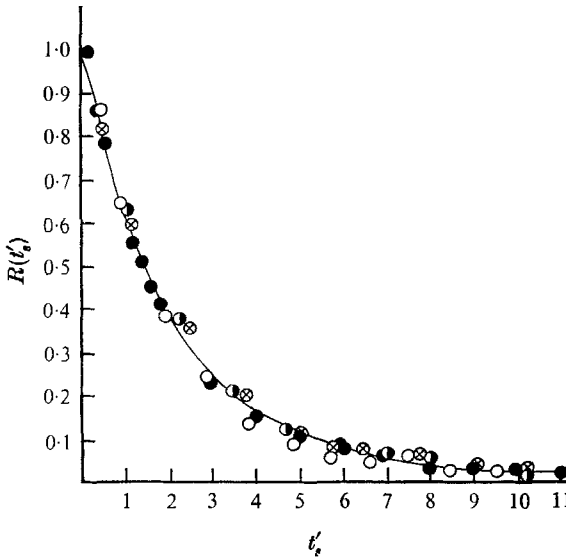
FIGURE 16. Comparison of simulation values of $R(t'_s)$ where t'_s represents t' scaled with respect to $(\overline{U}/u_*)^2$ using $R_* = 1000$ as a basis of comparison. Values of R_*: ⊗, 500; ◑, 1000; ●, 1500; ○, 2000.

Thus A_3 is approximately 11 if the simulated value of b, obtained at $R_* = 500$ is used. The integrated value is a constant and is independent of R_* for the universal curves selected in the simulation. In §2.2 the suggestion was made that A_3 should be a linear function of $(\overline{U}/u_*)^2$ and that the extremum functions would change accordingly with R_*. It was found in the simulation that, by rescaling the time variable t' by a factor $(\overline{U}/u_*)^2$, a similarity with respect to R_* is nearly realized.
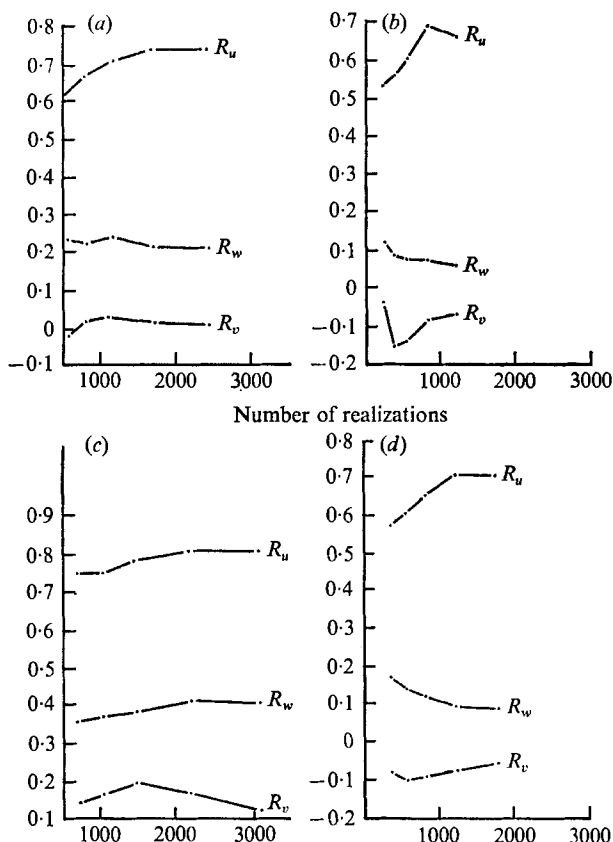
FIGURE 17. Convergence of experimental correlation values. $R_\phi = \overline{\phi'(t')\phi'(t'+\tau)}/\overline{\phi'(t')^2}$, $\phi = u, v, w$. (a) $t' = 0\cdot25$; (b) $t' = 1\cdot0$; (c) $t' = 0\cdot5$; (d) $t' = 0\cdot75$.

In figure 15, the compilation of the correlation function from the simulation is compared with the derived expression. In figure 16, the correlation functions determined from the simulation and scaled with respect to $(\overline{U}/u_*)^2$ appear to collapse onto a common curve thereby illustrating the R_* similarity with this scaling.

The numerical simulation appears to confirm the suggestion that extremum curves may be compiled in a piecewise manner, from observations over a relatively short time interval, and that the Lagrangian autocorrelation function, on the streamwise velocity, may be derived from the extremum curves of U^+.

4.3. Experiment

A photographic system was used to record the motion of neutrally buoyant ($\sim \frac{1}{2}$ mm diameter) spheres in the open channel flow described in §2.3. The system was capable of recording the motions at discrete time intervals of 0·07 sec. The photographic apparatus was made to move along the channel at a steady speed equal to the mean flow velocity. It consisted of a 35 mm camera, with a continuously advancing film, which recorded directly the plan view of the motion,
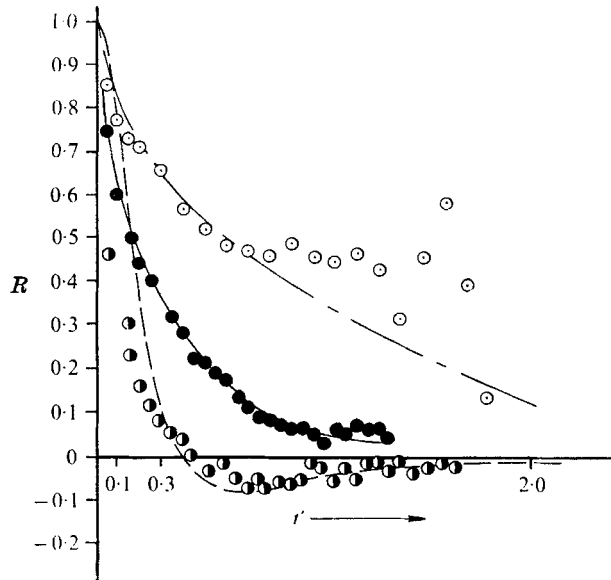

FIGURE 18. Measured Lagrangian autocorrelation functions. ●, $R = R_w$; ◑, $R = R_v$; ⊙, $R = \overline{(U(y') - u'(t'))\ (U(y') - u'(t' + \tau))}/\overline{(U(y) - u'(t'))^2}$; – – –, v' correlation found in simulation.
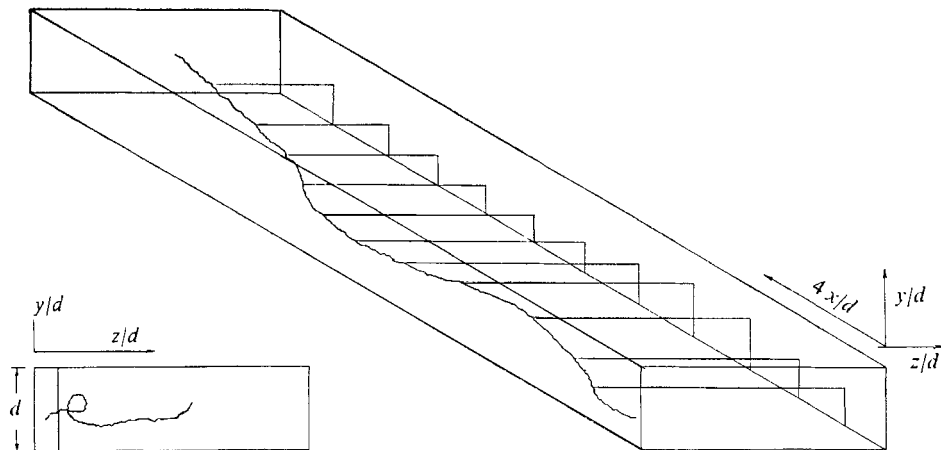
FIGURE 19. A typical particle path measured in experiment.

and recorded the elevation view via a series of mirrors. The particles were painted white, the channel boundaries matt black, and by using a rotating, slotted disk in place of the usual camera shutter, two series of dots were simultaneously exposed, on different halves of the film. From fiducial marks along the channel floor and short pulses of light that were introduced at regular intervals, the means were available for a continuous calibration of the various scale speeds and lengths. The three-dimensional motion, along with calibration data for each particle-passage along the flume, was recorded on a 30 cm length of 35 mm film. Information from the film record was transferred to digital format and subsequently stored on magnetic tape within the Titan digital-computer system used at Cambridge.
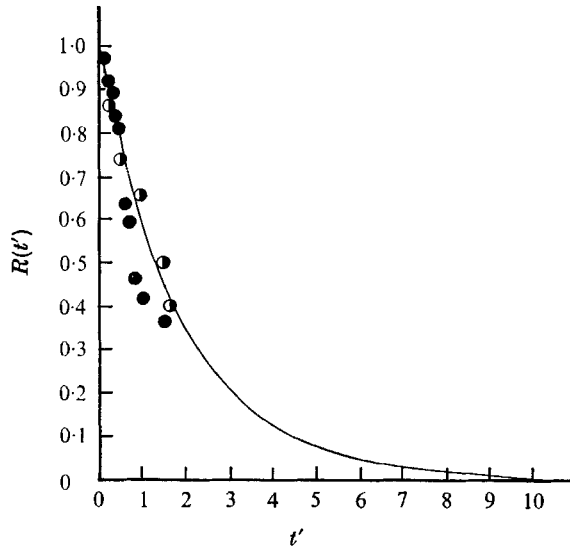
FIGURE 20. Experimental and simulated values of $R(t')$. ◑, experimental values $R_* = 620$; ●, experimental values $R_* = 620$ using measured extremum data; —, simulation result at $R_* = 500$.

There were 150 records of particle trajectories used in the analysis. Figure 17 indicates how the statistics converge as a function of the number of realizations for typical values of t' used in the correlation. No systematic error was found to occur in the data reduction over the depth of the channel; the estimated error is approximately 10 to 20 % of the lateral and longitudinal root-mean-square velocity and approximately 10 to 50 % of the value of the root-mean-square vertical velocity, for the respective velocity-component measurements. The experimental procedure is discussed in detail by Sullivan (1968).

The measured Lagrangian autocorrelation of the fluctuating cross-stream and streamwise velocity components are presented in figure 18. The streamwise correlation appears to fall off at a slower rate than the lateral and vertical equivalents, and hence exhibits a qualitative agreement with the Eulerian correlation of these fluctuating velocities. A typical particle path in the turbulent shear flow is shown in figure 19 and the 'eddy like' swirls in this path give one a sense of the 'length scale' of the fluctuating motion.
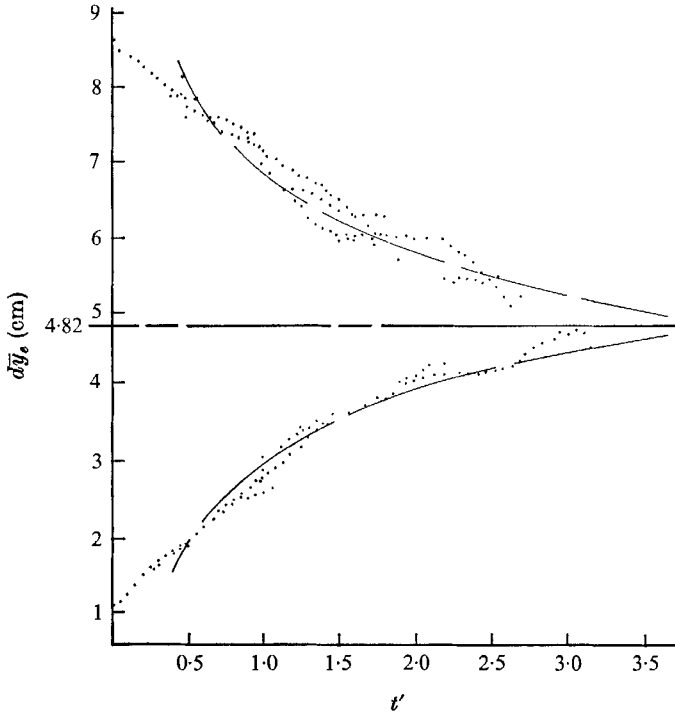
FIGURE 21. Experimental values for y'_e. ●, experimental result for various release positions on flow cross-section; − −, simulation result, $R_* = 500$.
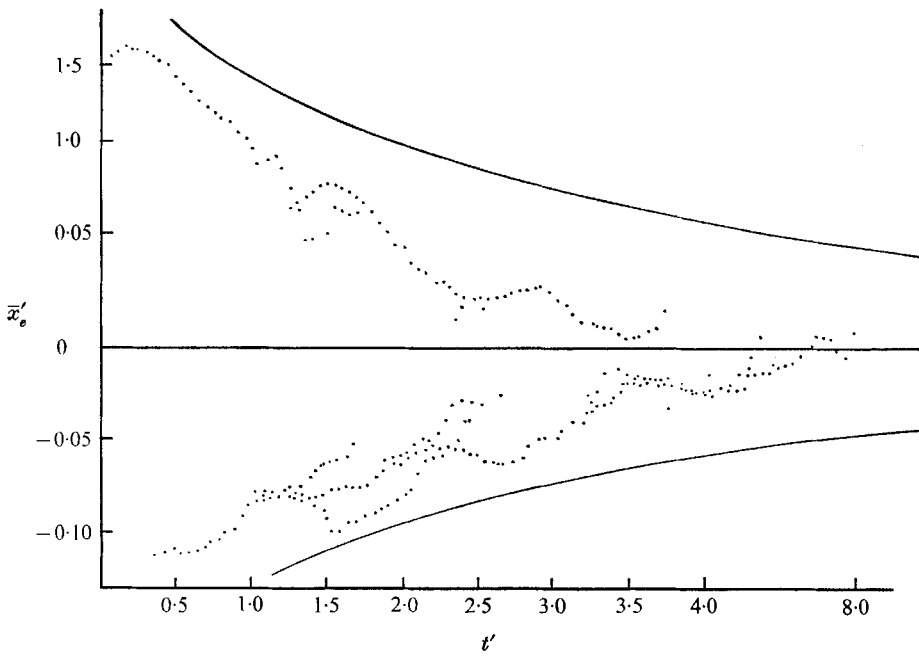

FIGURE 22. Experimental values for $\bar{x}'_e$. See figure 21 for symbols.

The measured autocorrelation of U^+ and of u' is compared in figure 20 with the result of simulation. Over the time interval for which the statistics are reliable (viz. $t' < 1$), there is little apparent difference between the autocorrelations using the measured data in these two ways. The time scale in the figure was not altered to account for the small difference of R_* between the simulation and experiment ($R_* = 500$ and 600 respectively) since a 1 % error in the value of the mean flow velocity would be as significant as this effect.
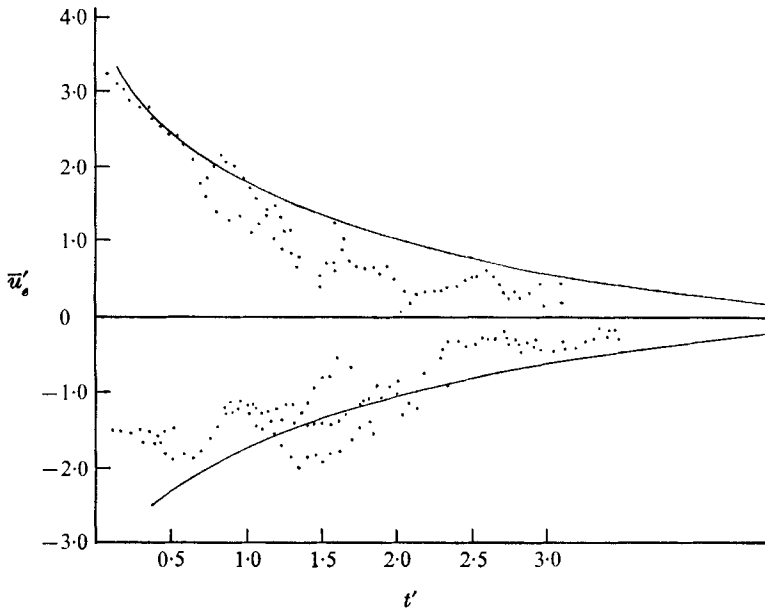

FIGURE 23. Experimental values for $\bar{u}'_e$. See figure 21 for symbols.

Figure 21 shows that the extremum path, compiled from the data by superposing path segments from 12 starting positions on the flow cross-sections, is in reasonable agreement with the simulation result. The existence of this extremum path immediately implies the existence of u'_e and X'_e. Measured extremum curves for u'_e and X'_e are compared in figures 22 and 23 with the simulation results. The data for u'_e and X'_e though not as complete as for y'_e, appears to confirm the general trend.

REFERENCES

BATCHELOR, G. K., BINNIE, A. M. & PHILLIPS, O. M. 1955 *Proc. Phys. Soc.* B **68**, 1095.

BENTLEY, P. G. & DAWSON, D. G. 1966 *Trans. Soc. Instrument Tech.* **18**, 183.

CLAUSER, F. H. 1956 *Adv. Appl. Mech.* **4**, 1.

ELDER, J. W. 1959 *J. Fluid Mech.* **5**, 544.

LAUFER, J. 1951 *NACA Rep.* no. 1033.

SULLIVAN, P. J. 1968 Ph.D. Thesis, Cambridge University.

TAYLOR, G. I. 1921 *Proc. London Math. Soc.* series 2, **20**, 196.

TAYLOR, G. I. 1953 *Proc. Roy. Soc.* A **219**, 186.

TAYLOR, G. I. 1954 *Proc. Roy. Soc.* A **223**, 446.

TOWNSEND, A. A. 1956 *The Structure of Turbulent Shear Flow.* Cambridge University Press.

$$tu^*/d = 0 \cdot 553$$
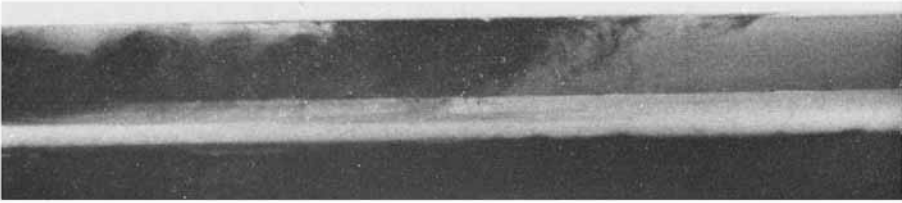
$$tu^*/d = 1 \cdot 06$$
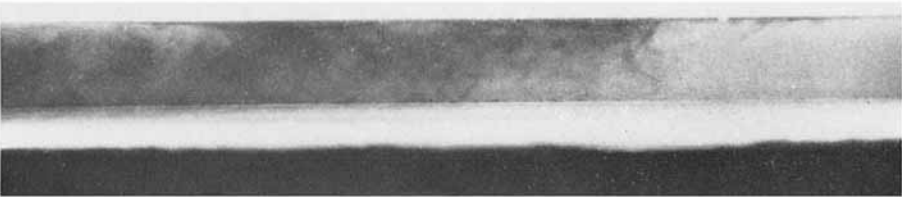
$$tu^*/d = 1 \cdot 64$$

FIGURE 1. Dispersing dye viewed through glass side walls of channel. $R_* = 784$.